

UC Berkeley

UC Berkeley Previously Published Works

Title

Relative Nucleus Pulposus Area and Position Alters Disc Joint Mechanics

Permalink

<https://escholarship.org/uc/item/6jm1282h>

Journal

Journal of Biomechanical Engineering, 141(5)

ISSN

0148-0731

Authors

Yang, Bo
Lu, Yintong
Um, Colin
[et al.](#)

Publication Date

2019-05-01

DOI

10.1115/1.4043029

Peer reviewed

Intervertebral Disc Mechanics with Nucleotomy: Differences between Simple and Complex Loading

Bo Yang, Ph.D..¹, Eric Klineberg, MD², Grace D. O'Connell, Ph.D.^{1,3}

¹Department of Mechanical Engineering,
University of California Berkeley,
Etcheverry Hall, Berkeley, CA, 94720

²Department of Orthopaedic Surgery
University of California, Davis
Davis Medical Center
Sacramento, CA, 95817

³Department of Orthopaedic Surgery
University of California, San Francisco
San Francisco, CA, 94142

Submitted to: Journal of Biomechanical Engineering

Corresponding Author:
Grace D. O'Connell, Ph.D.
University of California, Berkeley
Department of Mechanical Engineering
5122 Etcheverry Hall, #1740
Berkeley, CA 94720
ph: 510-642-3739
fx: 510-643-5539
Email: g.oconnell@berkeley.edu

1 **Abstract**

2 Painful herniated discs are treated surgically by removing extruded nucleus pulposus (NP)
3 material (nucleotomy). NP removal through enzymatic digestion is also commonly performed to
4 initiate degenerative changes to study potential biological repair strategies. Experimental and
5 computational studies have shown a decrease in disc stiffness with nucleotomy under single
6 loading modalities, such as compression-only or bending-only loading. However, studies that
7 apply more physiological loading conditions, such as compression in combination with bending
8 or torsion, have shown contradicting results. We used a previously validated bone-disc-bone finite
9 element model (Control) to create a Nucleotomy model to evaluate the effect of dual loading
10 conditions (compression with torsion or bending) on intradiscal deformations. While disc joint
11 stiffness decreased with nucleotomy under single loading conditions, as commonly reported in the
12 literature, dual loading resulted in an increase in bending stiffness, agreeing with clinical
13 observations. More specifically, dual loading resulted in a 40% increase in bending stiffness under
14 flexion and extension and a 25% increase in stiffness under lateral bending. The increase in
15 bending stiffness was due to an increase and shift in compressive stress, where peak stresses
16 migrated from the NP-annulus interface to the outer annulus. In contrast, the decrease in torsional
17 stiffness was due to greater fiber reorientation during compression. In general, large radial strains
18 were observed with nucleotomy, suggesting an increased risk for delamination or degenerative
19 remodeling. In conclusion, the effect of nucleotomy on disc mechanics depends on the type and
20 complexity of applied loads.

21 **Keyword:** Nucleus pulposus, Intervertebral disc, Nucleotomy, Finite element method,
22 Degeneration

1 **1. Introduction**

2 Partial removal of the nucleus pulposus (NP) is performed clinically to treat painful
3 herniated discs [1]. NP removal through enzymatic digestion is also performed to develop injury
4 or degeneration models to evaluate biological repair strategies. Experimental and computational
5 studies showed that NP removal affects disc joint mechanics and intradiscal deformations.
6 Nucleotomy decreases disc joint stiffness in torsion, bending, and shear, resulting in an increase
7 in range of motion and contact forces at the facet joints [2, 3]. Internally, nucleotomy decreases
8 intradiscal pressure under compression, resulting in inward bulging of the inner AF and greater
9 maximum AF strains [4-9]. However, most of these studies evaluated disc joint mechanics under
10 single loading modalities, such as compression- or bending-only loading, which is not
11 representative of complex *in vivo* loading conditions.

12 Few studies have evaluated disc mechanics under complex loading conditions. Previous
13 work showed that disc joint torsional and shear stiffness is dependent on the compressive preload
14 [10-14]. Recent studies that have applied complex six degrees of freedom loading have been
15 successful in initiating disc failure in intact discs [15, 16]. These findings have been valuable for
16 directing computational models [17]; however, quantifying the role of each loading modality to
17 failure has been difficult due to the wide range of loading configurations applied simultaneously.

18 Moreover, there have been limited research investigating the effect of nucleotomy on disc
19 mechanics with contradicting results. Nucleotomy has been reported to decrease disc shear
20 stiffness and increase loading on the facet joint and ligaments [13, 18]. Frei and coworkers showed
21 that nucleotomy increased extension stiffness, but did not affect flexion or lateral bending stiffness
22 [19]. Similar to Frei *et al.*, Shirazi-Adl and coworkers found that removing NP fluid increased
23 extension stiffness, but there was a marked decreased in flexion and rotation stiffness [20]. Lastly,

1 changes in lateral bending stiffness were found to be dependent on the amount of NP fluid removed
2 [20].

3 Therefore, the aim of this study was to evaluate the effect of nucleotomy on disc mechanics
4 using a finite element model of a bone-disc-bone motion segment that mimicked the anatomy of
5 human cadaver specimens prepared for experimental testing. The effect of single versus dual
6 loading on disc mechanics was evaluated. For dual loading conditions, axial compression was
7 applied as the primary loading configuration. Torsion, flexion, extension, or lateral bending was
8 applied after compression. We hypothesized that disc stiffness increases with nucleotomy when
9 tested under dual loading conditions, but will decrease under single loading conditions. To test this
10 hypothesis, we modified our previously-validated finite element model of the human lumbar disc
11 by removing the NP to create a total nucleotomy model [21]. Stiffness, internal stress, and strain
12 distributions was evaluated for multiple loading conditions.

13 **2. Method**

14 2.1. Model development

15 The Control model was a single bone-disc-bone motion segment with geometry based on
16 thirteen L3L4 human male discs averaged together (disc height = 11mm, disc area = 1949mm²,
17 NP area = 546mm², Figure 1) [21, 22]. The Control model included separate material descriptions
18 for the NP and AF, which were sandwiched between cartilage and bony endplates with thicknesses
19 of 0.8 mm and 0.6 mm, respectively (Figure 1) [23, 24]. The cartilage endplate covered the entire
20 NP and inner AF. Disc subcomponents and bones were welded together by sharing nodes at the
21 interface. The AF was divided into 20 concentric layers [25] and each layer was sub-divided into
22 four anatomical regions to assign region-dependent material properties [26, 27].

23 The NP, cartilage endplates, and AF matrix were described as isotropic hyperelastic
24 Mooney-Rivlin materials. The AF was described as having nonlinear tension-only elastic fibers

1 embedded within an extrafibrillar matrix. Material coefficients for NP, endplates, and AF matrix
2 were selected from the literature (Table 1) [28], while fiber coefficients were calibrated using data
3 from single lamellae tensile tests (Table 2) [26, 29]. Therefore, the outer AF was stiffer than the
4 inner AF and the anterior AF was stiffer than the posterior AF [26, 27]. A cross-ply fiber
5 architecture was defined, such that each adjacent lamellae had opposing fiber orientations. Fiber
6 orientation decreased from $\pm 43^\circ$ in the innermost layer to $\pm 28^\circ$ in the outermost layer [30]. The
7 cortical bone was described as a Neo-Hookean material (modulus = 12,000MPa, Poisson's ratio =
8 0.3) [28]. The NP was completely removed from the Control model to create the Nucleotomy
9 model, representing an extreme case of the nucleotomy procedure.

10 2.2. Model simulation and data analyses

11 Our previous study validated disc joint mechanics of the Control model by comparing
12 model results from single loading modalities (axial compression, torsion, flexion, extension, and
13 lateral bending) to experimental data [21]. In short, the normalized change in disc height under
14 axial compression and joint stiffness in bending agreed well with the literature [7, 10, 31].
15 Moreover, angular displacement-torque response in flexion, extension, lateral bending, and axial
16 rotation agreed well with the behavior reported in the literature [2, 32, 33].

17 Rigid bodies were in contact with the superior and inferior vertebral bodies. The inferior
18 rigid body was fixed in all degrees of freedom, while load and displacement were applied to the
19 superior rigid body, which was free to rotate. A 936N (0.48MPa) compressive load was applied
20 and angular displacements (4° in torsion, 6.5° in flexion, 4° in extension, or 5° in lateral bending,
21 based on data for human lumbar discs) was applied with free axes of rotation (2 models X 4
22 simulations = 8 total simulations) [34-36]. During bending or rotation, angular displacement about
23 the other axes was restricted. All simulations were conducted in FEBio [37].

1 The normalized change in disc height was calculated as displacement in the axial direction
2 divided by the initial disc height. Compressive stress was averaged across all elements in the disc
3 and plotted against the normalized change in disc height. Radial bulging was measured in the
4 anterior, lateral, and posterior AF at the mid-disc height. Peak stress, strain, and stretch were
5 calculated by sorting data for all elements and averaging the top 10%. Normalized compressive
6 stiffness (MPa) was calculated as the slope of the stress-normalized displacement curve in the toe
7 and linear regions. Torsional and bending stiffness (Nm/°) was calculated as the slope of the
8 torque-angular displacement curves. Stress and strain distributions were evaluated with respect to
9 the disc's natural axes (*i.e.*, axial, radial, and circumferential directions). Fiber stretch and
10 reorientation were calculated for each element, using the volume of each element as a weighting
11 factor. A weighted average was calculated for each AF layer, which included data from the anterior,
12 posterior, and lateral AF. The *volume ratio of stretched fibers* was defined the sum of element-
13 volumes with loaded fibers divided by the total element-volume for the layer.

14 **3. Result**

15 3.1 Disc joint mechanics: compression-only loading

16 The normalized change in disc height for the Nucleotomy model in axial compression was
17 2-fold greater than the Control model (2.63 mm or 23.9% versus 1.23 mm or 11.2%, Figure 2A).
18 Nucleotomy resulted in a 60% decrease in toe-region stiffness and a 40% decrease in linear-region
19 stiffness (Figure 2B). While a wide range of values for disc joint compressive modulus has been
20 published for intact (4-25 MPa) and partial or complete nucleotomy (2-29 MPa) [38], the relative
21 trends were comparable to behaviors reported in the literature (based on averaged data from the
22 literature) [2]. Thus, we considered the Nucleotomy model valid for assessing changes in
23 intradiscal stress and strain distributions.

1 Radial bulging was outward in the anterior (2.1 mm at the mid-disc height), posterior (1.8
2 mm), and lateral AF (1.4 mm). Nucleotomy resulted in a slight increase in the outward bulging of
3 the anterior AF (2.3 mm) and a 20% increase in outward bulging of the lateral AF. However,
4 outward bulging of the posterior AF was lower with Nucleotomy (1.4 mm versus 1.8 mm). In the
5 Control model, compression generated reaction torques of 2.20 Nm around the X-axis (flexion),
6 0.20 Nm around the Y-axis (lateral bending), and 0.09 Nm around the Z-axis (torsion). The
7 response was comparable for the Nucleotomy model, with reaction torques of 2.22 Nm, 0.28 Nm,
8 and 0.14 Nm around X-axis, Y-axis, and Z-axis, respectively.

9 3.2 Disc joint mechanics: dual loading conditions

10 While torque versus rotation for bending-only loading (*i.e.*, no compressive preload) was
11 nonlinear, a compressive preload resulted in linear torque-rotation behavior (Figure 3A). Torsional
12 stiffness decreased by more than 30% with nucleotomy. However, bending stiffness in flexion and
13 extension increased by more than 40% and lateral bending stiffness increased by 25% with
14 nucleotomy (Figure 3B). Since dual-loading conditions provide a better representation of *in vivo*
15 loading, further data analysis was performed on dual loading simulations, with compression-only
16 loading used for comparison.

17 Bending increased outward bulging on the side of loading (*e.g.*, anterior AF in flexion),
18 but decreased the magnitude of outward bulging on the opposite side. For example, under
19 extension, the Control model anterior AF bulging decreased by 60% (0.8 mm) and posterior AF
20 bulging increased by ~30% (2.3 mm). Changes in outward radial bulging was more pronounced
21 with Nucleotomy. Under extension, there was a 65% decrease in the anterior AF radial bulge and
22 a 50% increase in the posterior AF radial displacement (2.1mm). Axial rotation combined with

1 compression resulted in minimal outward radial bulging for all annular regions in both models
2 (bulge = 0.2 - 0.5 mm).

3 3.3 Stress distributions

4 In the Control model, axial compressive stress at the mid-transverse plane was greatest in
5 the NP (NP: 0.63 MPa versus AF: <0.5 MPa; Figure 4A). Peak axial compressive stresses in the
6 AF shifted towards the outer posterolateral region with Nucleotomy, with a 57% increase in stress
7 magnitude (Control = 0.51 MPa and Nucleotomy = 0.80 MPa; Figure 4A - 1st column). Applying
8 torsion after compression did not alter axial stress distributions in either the Control or Nucleotomy
9 model (Figure 4A – 1st column versus 2nd column). Flexion, extension, and lateral bending
10 combined with compression shifted the location of peak axial compressive stress towards the side
11 of loading (Figure 4A - 3rd -5th columns). In the Control model, peak axial compressive stresses
12 were located in the inner or inner-middle AF. Removal of the NP slightly shifted the location of
13 peak axial compressive stresses to the outer AF, resulting in a 50% increase in peak stress (0.89
14 MPa to 1.36 MPa).

15 In the Control, the NP experienced high compressive stress in the radial and circumferential
16 directions (magnitude > 0.5 MPa, Figures 4B & C – 1st and 3rd rows). The median radial-direction
17 stress in the NP was -0.59 MPa (peak = -0.64 MPa). Similar to axial-direction compressive stress,
18 bending resulted in a shift in the location of peak radial- and circumferential-direction stress and a
19 slight increase in peak stress magnitude (5% increase). In the Nucleotomy model, peak
20 compressive radial- and circumferential-direction stress occurred in the mid-AF and was located
21 on the side of bending load (Figures 4B & C – 3rd – 5th columns). In both Control and Nucleotomy
22 models, tensile circumferential direction stresses in the outer AF increased with bending and
23 torsion (Figure 4C – red regions) and greater tensile stresses occurring in the Control disc.

1 3.4 Strain distributions

2 In the Control model, axial direction strains under compression were similar in the NP and
3 AF, where peak compressive axial strains occurred at the mid-disc height (Figure 5A – 1st column).
4 NP removal resulted in greater compressive axial strains in the AF, with inward bulging of the
5 inner annulus, with peak strains remaining at the mid-disc height (Figure 5A - 1st column).
6 Applying torsion after compression did not alter axial strain maps (Figure 5A - 1st column versus
7 2nd column). Flexion, extension, and lateral bending in the Control model shifted the location of
8 peak compressive axial strains to the side of loading, while the opposite side experienced tensile
9 axial strains (*e.g.*, posterior AF under flexion; Figure 5A - columns 3-5, top row). In contrast, peak
10 tensile and compressive axial strains in the Nucleotomy model occurred on the same side as
11 loading (Figures 5A - columns 3-5, bottom row).

12 Due to the Poisson effect, large tensile radial strains developed at the location of peak
13 compressive axial strains (Figure 5B). Similarly, large compressive radial strains developed at
14 locations of tensile axial strains. Lastly, the magnitude of circumferential strains was much lower
15 (<25%) than the magnitude of axial or radial strains (<0.1 versus <0.4MPa; Figure 5C). In the
16 Control model, tensile circumferential direction strains were higher in the NP. With Nucleotomy,
17 tensile circumferential direction strains only developed as localized strain concentrations at the
18 innermost (*i.e.*, extension) or outermost AF regions (*e.g.*, flexion or lateral bending).

19 3.5 Fiber stretch

20 In the Control model, 35% of inner AF fibers (*i.e.*, stretch volume ratio ≈ 0.35) and $\sim 85\%$
21 of outer AF fibers were loaded in tension during compression (Figure 6A – black, Figure 7A - 1st
22 column). Nucleotomy decreased fiber engagement in the inner AF under compression, with only
23 20% of inner AF fibers loaded in tension. However, fiber engagement in the outer AF was not

1 affected by Nucleotomy (Figure 6A – blue). In the Control, fibers that were engaged during
2 compression experienced relatively uniform stretch throughout the AF (average stretch ~1.02;
3 Figure 6B). Layer-averaged fiber stretch in the inner AF increased 2-3-fold with nucleotomy
4 (Figure 6B – black versus blue ‘x’s).

5 Applying torsion after compression resulted in total fiber engagement in every other layer,
6 where fibers were more aligned with the rotation direction, while fibers in adjacent layers were
7 not loaded (Figure 6C). Engagement of only half of the available fibers during torsion resulted in
8 an increase in fiber stretch from 1.02 to over 1.04 (Figure 6B versus 6D), where peak fiber stretch
9 occurred in the posterior and posterior-lateral AF (Figure 7A - 2nd column). With Nucleotomy,
10 fiber engagement under torsion followed a similar trend, but maximum fiber engagement in the
11 inner AF was 40% lower than the Control (Figure 6C), resulting in slight differences in fiber stretch
12 (Figure 6B versus 6D – blue lines). Nucleotomy did not alter fiber engagement and stretch in the
13 outer AF during torsion with compression.

14 Fiber engagement during bending with compression was relatively uniform throughout the
15 AF, increasing in the outer 25% of the annulus (Figure 6E). Bending increased inner AF fiber
16 engagement by 50% in the Control. Similarly, in the Nucleotomy model, inner and mid-AF fiber
17 engagement increased from relatively no fiber engagement to 20% of fibers being loaded (Figure
18 6A versus 6E – blue lines) Although the Control model had a greater percentage of loaded fibers
19 throughout the AF, the average fiber stretch of loaded fibers was less than 1.06 and was not
20 affected by Nucleotomy (Figure 6E-F). Fiber stretch in the Control was greatest in the anterior-
21 lateral to lateral AF for all loading configurations with peak values less than 1.08 (Figure 7A - 3rd
22 – 5th columns). However, the location of peak fiber stretch shifted to the side of bending with
23 Nucleotomy (Figure 7A – bottom row, columns 3-5). Thus, peak fiber stretch occurred in the

1 posterior AF under extension and the anterior AF under flexion, and peak fiber stretch was slightly
2 higher with Nucleotomy (<1.11).

3 3.6 Fiber reorientation

4 Under axial compression, fibers reoriented towards the transverse plane; however, the
5 magnitude of fiber reorientation was 2X greater with Nucleotomy ($\sim 10^\circ$ versus $\sim 5^\circ$; Figure 8A).
6 Furthermore, more fiber reorientation occurred in the posterior AF with Nucleotomy (Figure 7B –
7 1st column). Torsion resulted in a zig-zagged pattern in layer-averaged fiber reorientation, where
8 AF layers with greater fiber stretch corresponded to layers with more fiber reorientation (Figures
9 6D & 8B). Bending resulted in relatively few changes in fiber reorientation (Figure 8A), but
10 region-dependent changes were observed in both models (Figure 7B - 3rd – 5th columns). For
11 example, flexion increased fiber reorientation in the anterior AF and decreased fiber reorientation
12 in the posterior AF (Figure 7B – 1st versus 3rd column). Lastly, fibers in the inner AF of the
13 Nucleotomy model reoriented away from the transverse plane, likely due to inward bulging of the
14 AF (Figure 7B).

15 **4. Discussion**

16 Simulations showed that the effect of nucleotomy on disc joint mechanics depended on
17 whether single or multi-loading modalities were considered. Under compression- or bending-only
18 loading, nucleotomy decreased stiffness, agreeing with previous experimental and computational
19 studies [2, 3, 5, 6, 32, 39]. However, dual loading, such as compression combined with bending,
20 resulted in an increase in bending stiffness, suggesting that the disc is more resistant to bending
21 after nucleotomy. The discrepancy between single- and dual-loading highlights the importance of
22 evaluating disc joint mechanics under conditions that better represent *in vivo* loading [15, 17]. A
23 recent review of the spine biomechanics literature highlighted the range and use of compressive

1 preloading prior to bending, which leads to large differences in reported mechanical properties.
2 Moving towards consensus in mechanical testing methodologies will make comparing results
3 between studies easier [40]. However, this study shows how data from finite element models can
4 complement experimental findings and allow for comparisons to be made between specimens and
5 or different study designs [41].

6 The disc is often compared to a pressurized tire; however, the loss of NP pressure, either
7 through severe degeneration or nucleotomy, causes the disc to behave more like a compressed O-
8 ring with the AF absorbing much of the applied stress [42]. The Nucleotomy model demonstrated
9 greater outward bulging of the outer AF, larger tensile radial strains, and inward bulging of the
10 inner AF, agreeing well with experimental observations [5-7, 9, 43]. Large tensile radial strains
11 occurred more frequently in the mid-AF and may lead to annular delamination, which is known to
12 be more prevalent in older or degenerated discs [43-45]. Moreover, herniated discs have also been
13 shown to have thicker lamellae, which may be a result of a tissue remodeling or permanent
14 deformations from larger radial tensile strains [43, 46, 47].

15 The increase in joint stiffness with bending was largely due to the applied load being placed
16 entirely on the AF, rather than being distributed between the AF and softer NP [7]. The healthy
17 intact disc acts as a moving pivot joint, with the pivot point located near the NP-AF interface in
18 the Control model. After nucleotomy, the pivot point shifted towards the outer AF, which may
19 contribute to disc joint instability. The shift in pivot point during bending also reflects a shift in
20 the concentration of applied stress. The increase in disc joint stiffness was largely due to greater
21 compressive stresses (~50% increase) and nonlinear material properties in the AF [26, 48]. Thus,
22 biological repair strategies that aim to restore NP function should act to re-shift the pivot point
23 towards the disc centroid or NP-AF interface [38, 49].

1 Generally, dual loading with Nucleotomy resulted in an increase in bending stiffness, but
2 joint stiffness decreased under axial rotation. Previous studies have shown that AF damage, as
3 observed in herniated discs, results in a decrease in axial rotation stiffness [50, 51, 52]. The loss in
4 torsional stiffness with annular injury was due to a reduction in fiber engagement, where only
5 fibers in alternating layers experience loading [Yang, 2017 #39]. This suggests that the
6 Nucleotomy model likely underestimated the decrease in torsional stiffness, due to the posterior-
7 lateral AF not being damaged in the model. Regardless, the findings from this study suggest that
8 the decrease in torsional stiffness was largely due to differences in behavior that occurred during
9 axial compression, where fibers reoriented towards the horizontal plane and the amount of fiber
10 reorientation increased with nucleotomy. Our previous work showed that discs with fibers
11 orientated closer to the horizontal plane have lower torsional stiffness and maximum shear strains
12 [29]. More importantly, a decrease in torsional stiffness has been shown to occur in patients with
13 lower back pain [53]. Taken together, this suggests that restoring torsional stiffness is an important
14 target for biological repair strategies [54].

15 Large differences were observed in fiber stretch and engagement (Figure 6). Fiber
16 engagement under compression or torsion decreased with Nucleotomy. Therefore, fibers that were
17 engaged during loading experienced greater strains (fiber stretch), which may make the inner AF
18 more susceptible to damage accumulation. This agrees well with observations of herniated discs
19 with more inner AF damage having a higher risk for re-herniation [55]. Thus, NP repair strategies
20 that re-pressurize the disc may act to decrease fiber stretch in the inner AF, reducing the risk of
21 additional AF damage [56].

22 Surgical treatment for painful disc herniation requires a balance between relieving pain,
23 reducing the risk of re-herniation, and minimizing the amount of material removed. In this study,

1 we evaluated an extreme case of nucleotomy; however, the actual amount of NP material removed
2 during surgery can vary widely based on injury severity, disc health, and surgeons' approach. In
3 healthy or moderately degenerated discs, the remaining NP may be able to swell further and
4 partially maintain disc function, but the decrease in intradiscal pressure may cause degenerative
5 changes, due to an increase in tensile radial strains [7].

6 The current model did not include facet joints or ligaments to evaluate disc joint
7 biomechanics and better represent *in vitro* experiments. Selection of incompressible or
8 compressible material descriptions affects predicted stress magnitudes [57]. We described the NP
9 and AF as having a compressible solid matrix [58], which may have predicted lower stresses and
10 higher strains than a model that describes the solid matrix as being incompressible [20]. Load-
11 controlled compression was applied to better represent *in vivo* loading (*i.e.*, muscle forces and
12 gravity); therefore, we assumed little to no change in muscle forces or body weight after
13 nucleotomy. Angular rotations were restricted during axial compression, which resulted in reacting
14 torques in both Control and Nucleotomy models. Thus, torque offset was subtracted to evaluate
15 bending and torsional stiffness. The Nucleotomy model did not describe AF damage that typically
16 occurs in the posterolateral region, which would affect the magnitude of predicted stresses and
17 strains near the injury site [38, 59]. Lastly, soft tissues in the model were described as hyperelastic
18 materials, which does not account for time dependent behaviors. Thus, understanding the effect of
19 nucleotomy on short-time scales (viscoelasticity) or long-time scales (tissue remodeling) could not
20 be assessed, but is an important area of study.

21 In conclusion, the effect of nucleotomy on disc mechanics was dependent on the type and
22 complexity of the applied loading condition. While disc joint stiffness decreased with nucleotomy
23 under single loading conditions, as commonly reported in the literature, dual-loading conditions

- 1 resulted in an increase in bending stiffness, agreeing with clinical observations. Dual loading with
- 2 nucleotomy resulted in an increase in strain magnitude and altered the distribution of AF stresses
- 3 and strains, which may lead to further damage accumulation and degenerative remodeling.

1 **5. Competing Interests**

2 We have no competing interests.

3

4 **6. Authors' Contributions**

5 Bo Yang and Grace D. O'Connell participated in study design, data analysis, data interpretation,
6 and manuscript writing. Eric Klineberg participated in data interpretation and manuscript writing.

7 Bo Yang performed all the simulations. All authors provided final approval for publication.

8

9 **7. Funding**

10 This work was supported by the Regent's of the University of California, the Signatures Innovation
11 Fellowship from the University of California, and the National Science Foundation (NSF
12 CAREER # 1751212).

13

- 1 **Table 1:** Material parameters for the nucleus pulposus (NP), extrafibrillar matrix of the annulus fibrosus
2 (AF), and cartilaginous endplate (CEP), which were described Mooney-Rivlin materials (c_1 , c_2 , k).

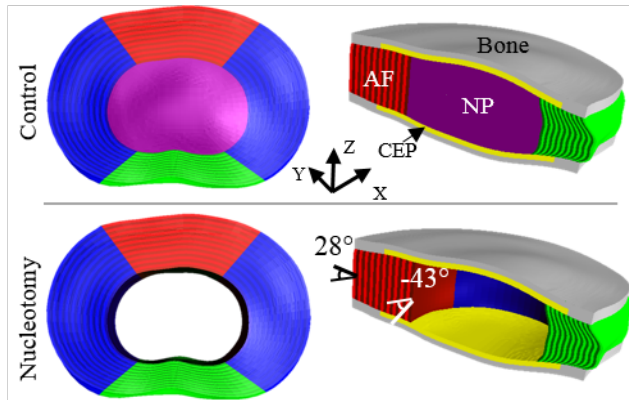
Property	NP	AF Matrix	CEP
c_1 (MPa)	0.05	0.09	0.55
c_2 (MPa)	0.01	0.01	0.01
k (MPa)	50	3	20

3

1 **Table 2:** Material coefficients for fibers in different regions of the annulus fibrosus. AO: anterior-outer, AI:
 2 anterior-inner, LO: lateral-outer, LI: lateral-inner, PO: posterior-outer, and PI: posterior-inner. Fibers were
 3 described using a nonlinear strain energy density function, where E represents the linear region Young's
 4 modulus, β represents toe-region nonlinearity, and λ_0 represents the transition stretch between the toe and
 5 linear region.

Region	AO	AI	PO	PI	LO	LI
E (MPa)	57	18	35	15	46	16.5
β	4	5	5	6	4.5	5.5
λ_0	1.01	1.07	1.03	1.10	1.02	1.09

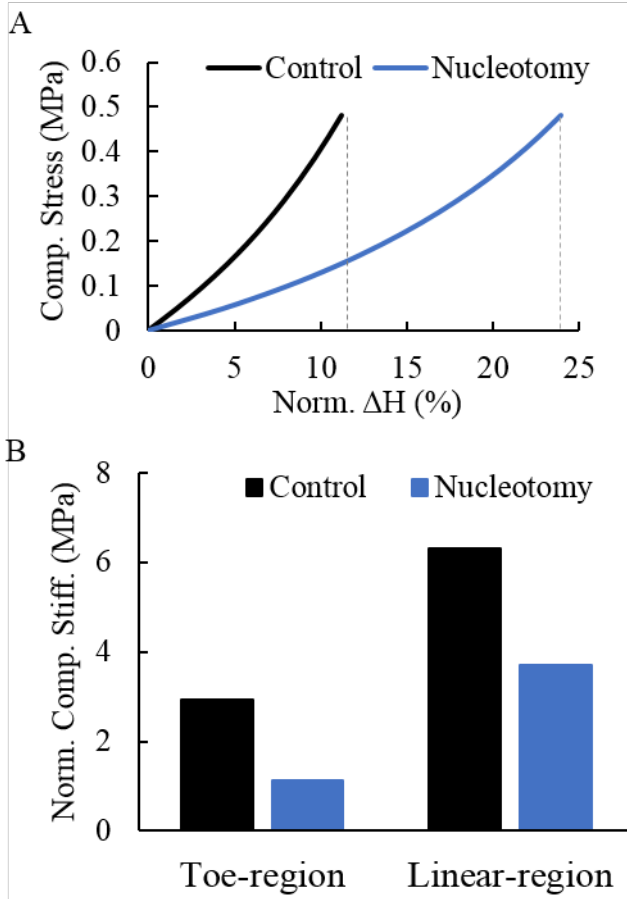
6



1

2 **Figure 1:** Schematic of Control and Nucleotomy models. The annulus fibrosus (AF) was separated
 3 into four anatomical regions (red = anterior, blue = lateral, and green = posterior). Fiber orientation
 4 alternated between layers, decreasing from $\pm 43^\circ$ with respect to the horizontal plane in the inner
 5 AF to $\pm 28^\circ$ in the outer AF. The model also included material descriptions for the nucleus pulposus
 6 (NP, purple, only in Control model), cartilaginous endplates (CEP, yellow), and bony endplates
 7 (grey).

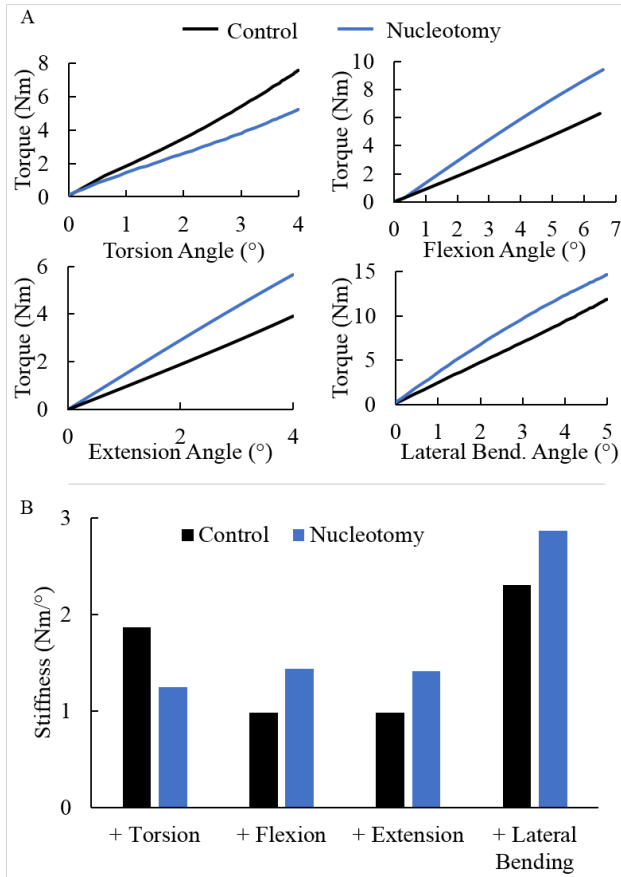
8



1

2 **Figure 2:** A) Compressive stress versus normalized change in disc height. B) Normalized
 3 compressive stiffness in the toe and linear regions, which was calculated as the slope of
 4 compressive stress versus normalized change in disc height.

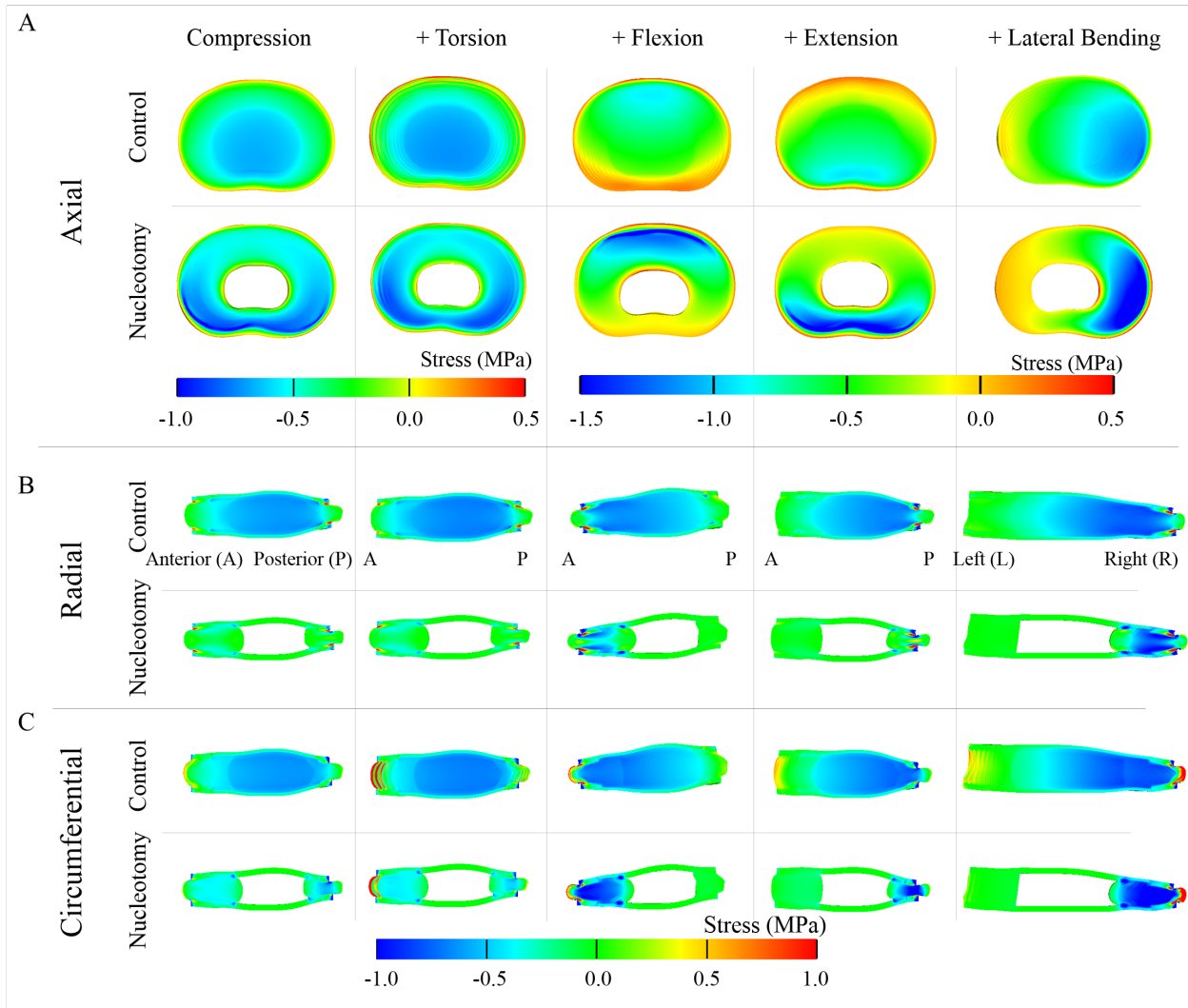
5



1

2 **Figure 3:** A) Torque versus rotation angle for Control (black) and Nucleotomy (blue) models
 3 under axial torsion, flexion, extension, and lateral bending. A 948 N compressive load was applied
 4 prior to bending. B) Disc joint stiffness was calculated as the slope of each torque-rotation curve.
 5 '+' for labels on the x-axis indicates that each loading condition was applied in combination with
 6 axial compression.

7

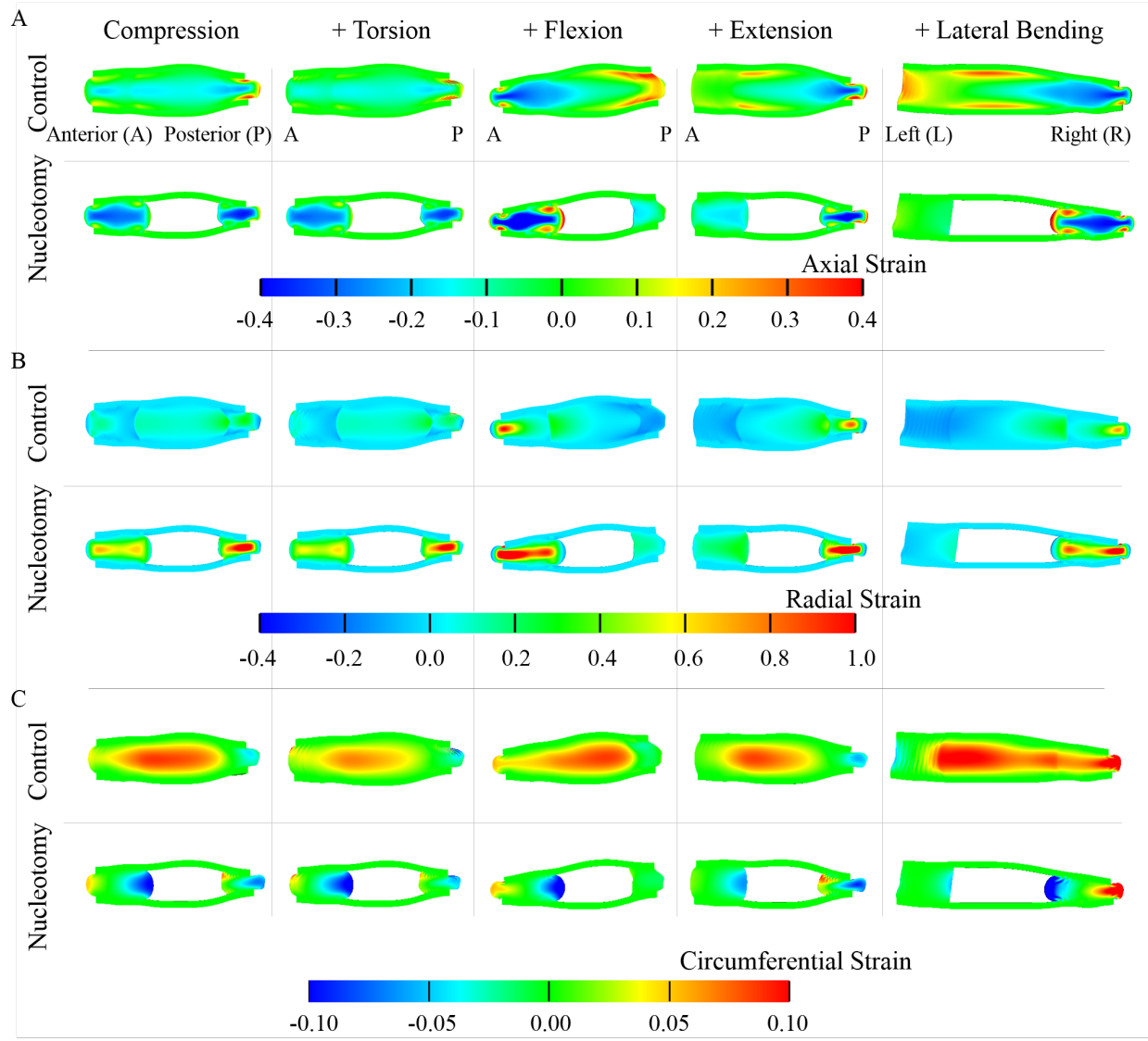


1

2 **Figure 4:** A) Axial stress distribution at the mid-transverse plane and B) radial and C)
 3 circumferential direction stress distributions at the mid-sagittal plane for Control (top row) and
 4 Nucleotomy (bottom) models. Axial torsion, flexion, extension, or lateral bending was applied
 5 after axial compression (denoted by '+'). Peak compressive stress was ~50% greater in flexion,
 6 extension, and lateral bending; therefore, a separate legend was used for clarity.

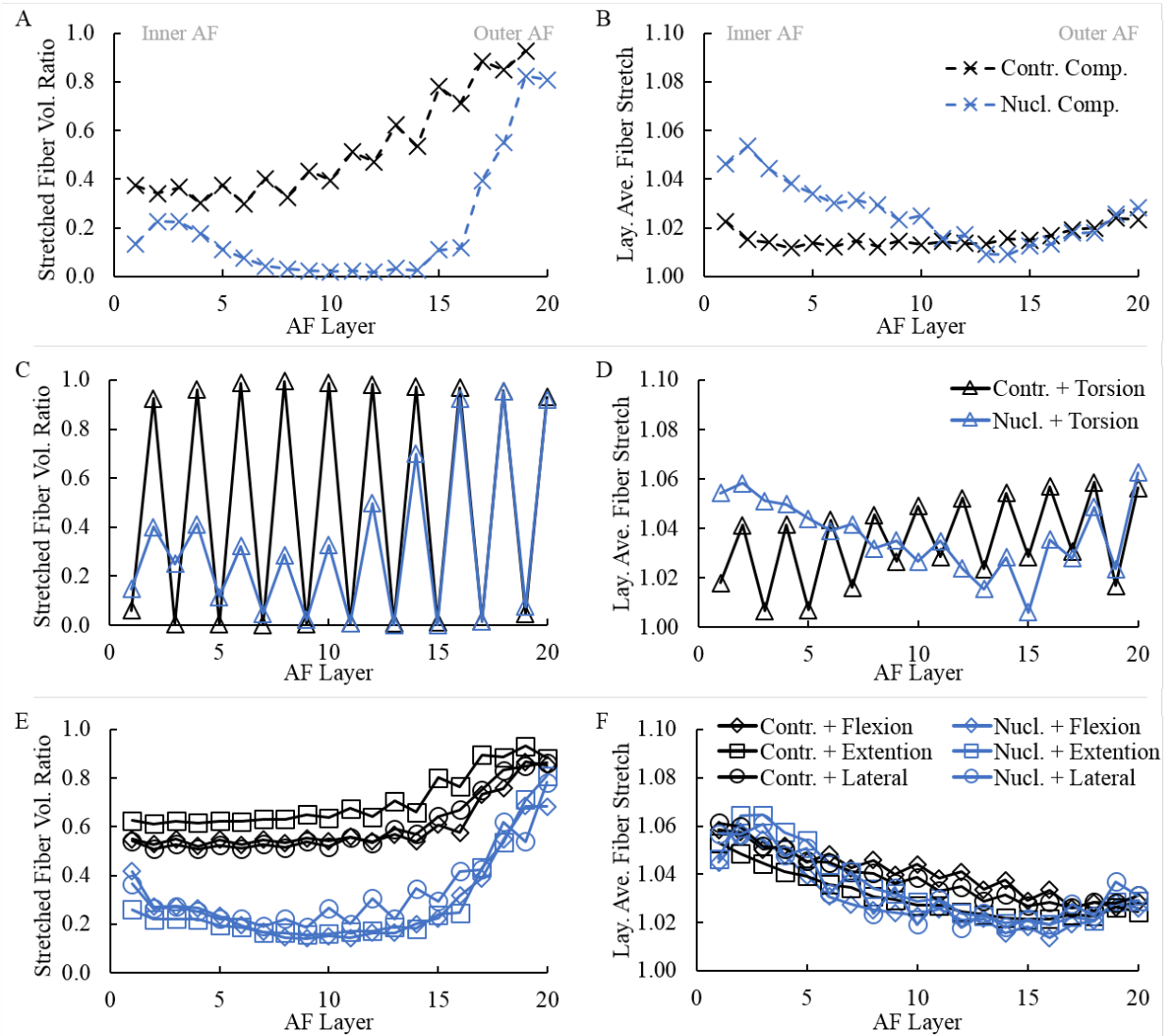
7

8



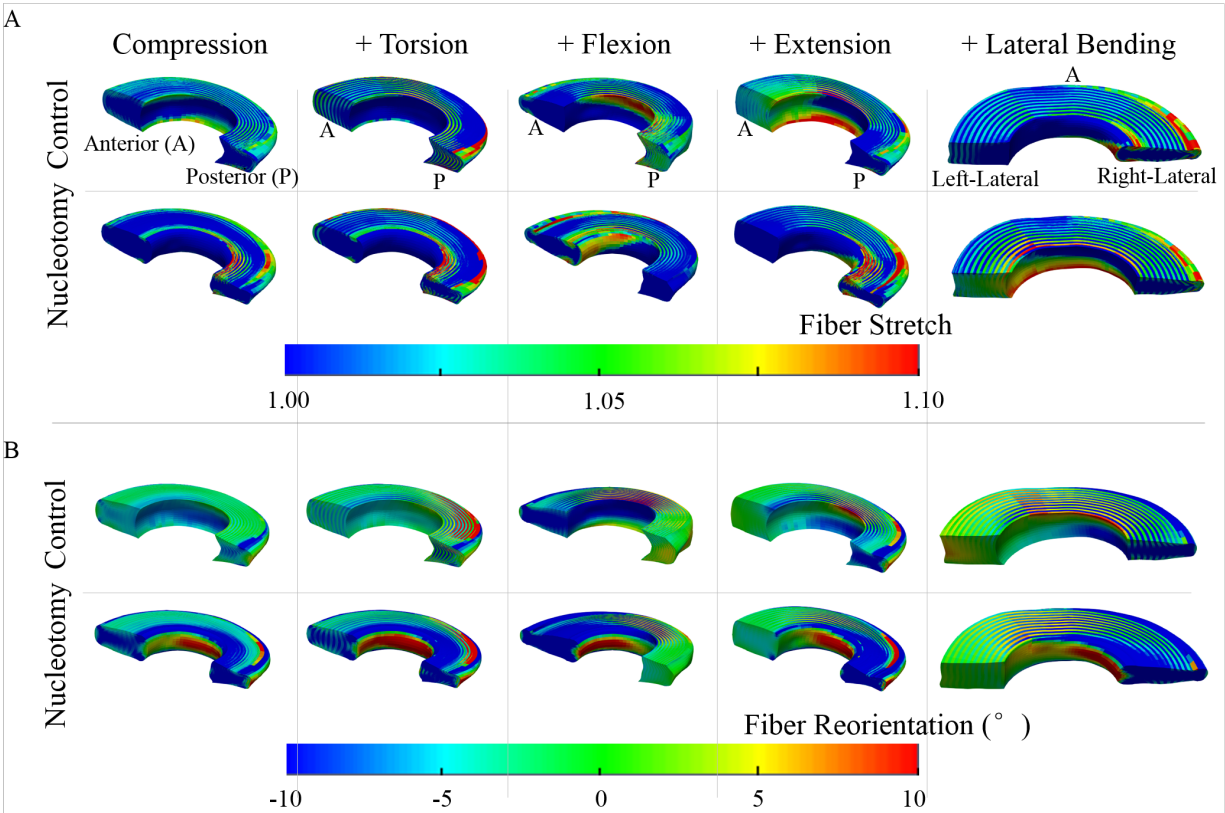
1
 2 **Figure 5:** A) Axial, B) radial, and C) circumferential strain distributions at the mid-sagittal plane
 3 for Control (top row) and Nucleotomy (bottom row) models. '+' indicates axial torsion, flexion,
 4 extension, or lateral bending was applied after compression.

5



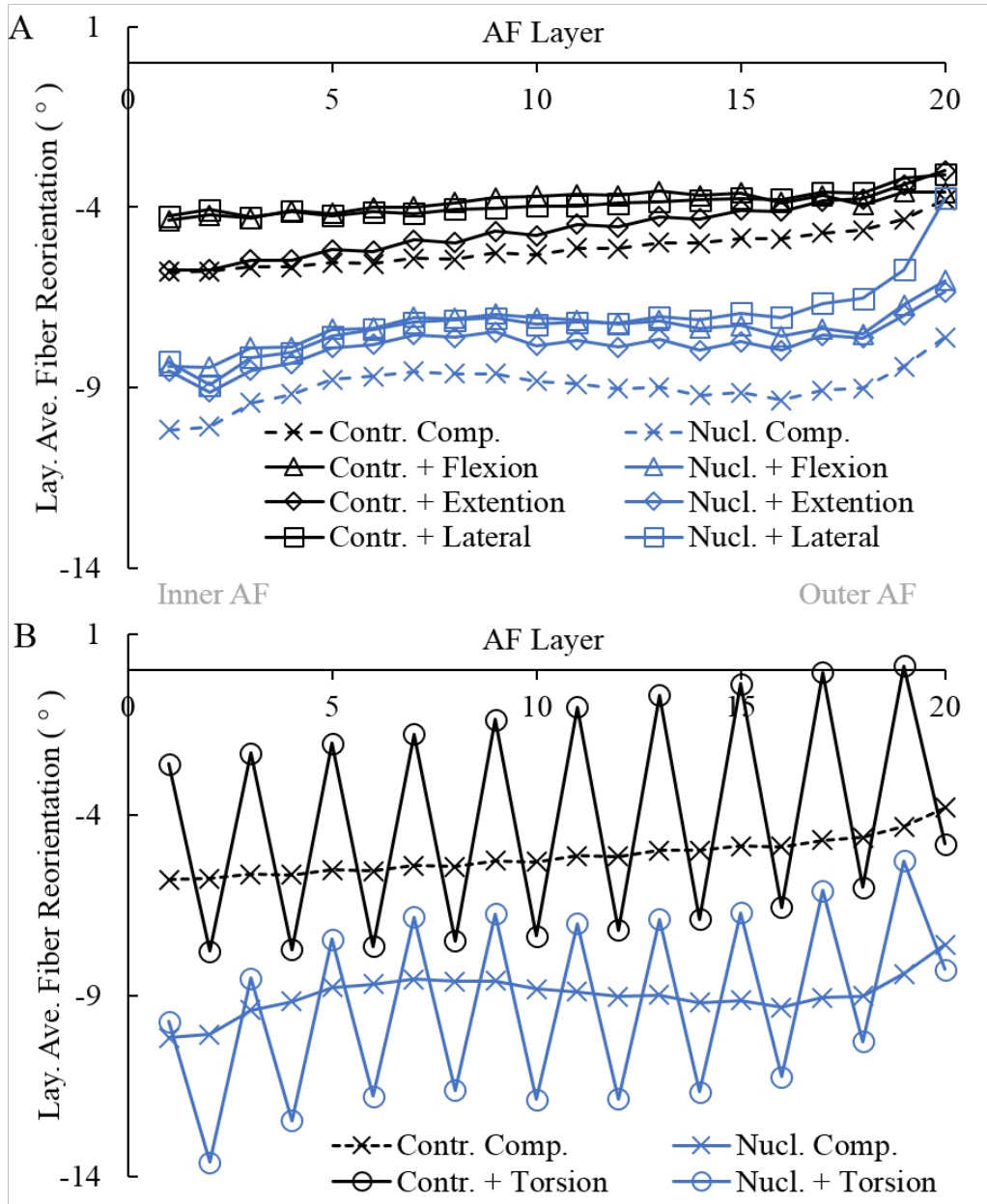
1
 2 **Figure 6:** Data shown in the left column represents volume ratio of fiber elements under tension
 3 for each lamellae, including data from the anterior, posterior, and lateral regions. Data shown in
 4 the right column represents layer-averaged fiber stretch with respect to lamellae layer. For all plots,
 5 Layer 1 represents the innermost layer and Layer 20 represents the outermost layer. Fiber stretch
 6 is shown for (A & B) compression-only loading, (C & D) compression with torsion, and (E & F)
 7 compression with bending. Black lines represent data the Control model and blue lines represent
 8 data from the Nucleotomy model. Figures in the same row shared the same legend.

9



1
 2 **Figure 7:** A) Fiber stretch and B) reorientation for the Control (top row) and Nucleotomy (bottom
 3 row) model under torsion, flexion, extension, and lateral bending, which was applied after axial
 4 compression (represented by '+'). Positive values represent fiber reorientation towards the axial
 5 plane, while negative values represent reorientation towards the transverse plane.

6



1
 2 **Figure 8:** Layer-averaged fiber reorientation for Control (black) and Nucleotomy (blue) models.
 3 A) Flexion (triangles), extension (diamonds), lateral bending (squares), and B) torsion (circles)
 4 was applied after axial compression. Positive values represent fiber reorientation towards the axial
 5 plane, while negative values represent reorientation towards the transverse plane.

6
 7
 8

1 8. Reference

- 2 [1] O'Connell, G. D., Leach, J. K., and Klineberg, E. O., 2015, "Tissue Engineering a Biological Repair
3 Strategy for Lumbar Disc Herniation," *BioResearch open access*, 4(1), pp. 431-445.
- 4 [2] Cannella, M., Arthur, A., Allen, S., Keane, M., Joshi, A., Vresilovic, E., and Marcolongo, M., 2008,
5 "The role of the nucleus pulposus in neutral zone human lumbar intervertebral disc mechanics," *Journal*
6 *of biomechanics*, 41(10), pp. 2104-2111.
- 7 [3] Huang, J., Yan, H., Jian, F., Wang, X., and Li, H., 2015, "Numerical analysis of the influence of
8 nucleus pulposus removal on the biomechanical behavior of a lumbar motion segment," *Computer*
9 *methods in biomechanics and biomedical engineering*, 18(14), pp. 1516-1524.
- 10 [4] Joshi, A. B., 2004, "Mechanical behavior of the human lumbar intervertebral disc with polymeric
11 hydrogel nucleus implant: an experimental and finite element study."
- 12 [5] Meakin, J., and Hukins, D., 2000, "Effect of removing the nucleus pulposus on the deformation of
13 the annulus fibrosus during compression of the intervertebral disc," *Journal of biomechanics*, 33(5), pp.
14 575-580.
- 15 [6] Meakin, J. R., Reid, J. E., and Hukins, D. W., 2001, "Replacing the nucleus pulposus of the
16 intervertebral disc," *Clinical biomechanics*, 16(7), pp. 560-565.
- 17 [7] O'Connell, G. D., Malhotra, N. R., Vresilovic, E. J., and Elliott, D. M., 2011, "The effect of discectomy
18 and the dependence on degeneration of human intervertebral disc strain in axial compression," *Spine*,
19 36(21), p. 1765.
- 20 [8] Seroussi, R. E., Krag, M. H., Muller, D. L., and Pope, M. H., 1989, "Internal deformations of intact
21 and denucleated human lumbar discs subjected to compression, flexion, and extension loads," *Journal of*
22 *Orthopaedic Research*, 7(1), pp. 122-131.
- 23 [9] Strange, D. G. T., Fisher, S. T., Boughton, P. C., Kishen, T. J., and Diwan, A. D., 2010, "Restoration
24 of compressive loading properties of lumbar discs with a nucleus implant—a finite element analysis
25 study," *The Spine Journal*, 10(7), pp. 602-609 %@ 1529-9430.
- 26 [10] Bezci, S. E., Eleswarapu, A., Klineberg, E. O., and O'Connell, G. D., 2018, "Contribution of facet
27 joints, axial compression, and composition to human lumbar disc torsion mechanics," *Journal of*
28 *orthopaedic research : official publication of the Orthopaedic Research Society*.
- 29 [11] Bezci, S. E., Klineberg, E. O., and O'Connell, G. D., 2018, "Effects of axial compression and rotation
30 angle on torsional mechanical properties of bovine caudal discs," *Journal of the mechanical behavior of*
31 *biomedical materials*, 77, pp. 353-359.
- 32 [12] O'Connell, G. D., Vresilovic, E. J., and Elliott, D. M., 2007, "Comparison of animals used in disc
33 research to human lumbar disc geometry," *Spine (Phila Pa 1976)*, 32(3), pp. 328-333.
- 34 [13] Schmidt, H., Bashkuev, M., Dreischarf, M., Rohlmann, A., Duda, G., Wilke, H. J., and Shirazi-Adl, A.,
35 2013, "Computational biomechanics of a lumbar motion segment in pure and combined shear loads," *J*
36 *Biomech*, 46(14), pp. 2513-2521.
- 37 [14] Shirazi-Adl, A., Ahmed, A. M., and Shrivastava, S. C., 1986, "Mechanical response of a lumbar
38 motion segment in axial torque alone and combined with compression," *Spine (Phila Pa 1976)*, 11(9), pp.
39 914-927.
- 40 [15] Amin, D., Lawless, I., Sommerfeld, D., Stanley, R., Ding, B., and Costi, J., 2016, "The effect of six
41 degree of freedom loading sequence on the in-vitro compressive properties of human lumbar spine
42 segments," *Journal of biomechanics*, 49(14), pp. 3407-3414.
- 43 [16] Berger-Roscher, N., Casaroli, G., Rasche, V., Villa, T., Galbusera, F., and Wilke, H.-J., 2017,
44 "Influence of complex loading conditions on intervertebral disc failure," *Spine*, 42(2), pp. E78-E85.

- 1 [17] Casaroli, G., Villa, T., Bassani, T., Berger-Roscher, N., Wilke, H.-J., and Galbusera, F., 2017,
2 "Numerical prediction of the mechanical failure of the intervertebral disc under complex loading
3 conditions," *Materials*, 10(1), p. 31.
- 4 [18] Ivicsics, M. F., Bishop, N. E., Puschel, K., Morlock, M. M., and Huber, G., 2014, "Increase in facet
5 joint loading after nucleotomy in the human lumbar spine," *J Biomech*, 47(7), pp. 1712-1717.
- 6 [19] Frei, H., Oxland, T. R., Rathonyi, G. C., and Nolte, L. P., 2001, "The effect of nucleotomy on lumbar
7 spine mechanics in compression and shear loading," *Spine (Phila Pa 1976)*, 26(19), pp. 2080-2089.
- 8 [20] Shirazi-Adl, A., 1992, "Finite-element simulation of changes in the fluid content of human lumbar
9 discs. Mechanical and clinical implications," *Spine (Phila Pa 1976)*, 17(2), pp. 206-212.
- 10 [21] Yang, B., Lu, Y., Um, C., and O'Connell, G., 2019, "Relative Nucleus Pulposus Area and Position
11 Alters Disc Joint Mechanics," *J Biomech Eng*.
- 12 [22] Peloquin, J. M., Yoder, J. H., Jacobs, N. T., Moon, S. M., Wright, A. C., Vresilovic, E. J., and Elliott,
13 D. M., 2014, "Human L3/L4 intervertebral disc mean 3D shape, modes of variation, and their relationship
14 to degeneration," *Journal of biomechanics*, 47(10), pp. 2452-2459.
- 15 [23] Moon, S. M., Yoder, J. H., Wright, A. C., Smith, L. J., Vresilovic, E. J., and Elliott, D. M., 2013,
16 "Evaluation of intervertebral disc cartilaginous endplate structure using magnetic resonance imaging," *Eur
17 Spine J*, 22(8), pp. 1820-1828.
- 18 [24] Rodriguez, A. G., Rodriguez-Soto, A. E., Burghardt, A. J., Berven, S., Majumdar, S., and Lotz, J. C.,
19 2012, "Morphology of the human vertebral endplate," *Journal of orthopaedic research : official
20 publication of the Orthopaedic Research Society*, 30(2), pp. 280-287.
- 21 [25] Marchand, F., and Ahmed, A. M., 1990, "Investigation of the laminar structure of lumbar disc
22 annulus fibrosus," *Spine*, 15(5), pp. 402-410.
- 23 [26] Holzapfel, G. A., Schulze-Bauer, C., Feigl, G., and Regitnig, P., 2005, "Single lamellar mechanics of
24 the human lumbar annulus fibrosus," *Biomechanics and modeling in mechanobiology*, 3(3), pp. 125-140.
- 25 [27] Skaggs, D. L., Weidenbaum, M., Iatridis, J. C., Ratcliffe, A., and Mow, V. C., 1994, "Regional
26 variation in tensile properties and biochemical composition of the human lumbar annulus fibrosus," *Spine*,
27 19(12), pp. 1310-1319 %@ 0362-2436.
- 28 [28] Dreischarf, M., Zander, T., Shirazi-Adl, A., Puttlitz, C., Adam, C., Chen, C., Goel, V., Kiapour, A., Kim,
29 Y., and Labus, K., 2014, "Comparison of eight published static finite element models of the intact lumbar
30 spine: predictive power of models improves when combined together," *Journal of biomechanics*, 47(8),
31 pp. 1757-1766.
- 32 [29] Yang, B., and O'Connell, G. D., 2017, "Effect of collagen fibre orientation on intervertebral disc
33 torsion mechanics," *Biomechanics and modeling in mechanobiology*, 16(6), pp. 2005-2015 %@ 1617-7959.
- 34 [30] Cassidy, J., Hiltner, A., and Baer, E., 1989, "Hierarchical structure of the intervertebral disc,"
35 *Connective tissue research*, 23(1), pp. 75-88.
- 36 [31] Beckstein, J. C., Sen, S., Schaer, T. P., Vresilovic, E. J., and Elliott, D. M., 2008, "Comparison of
37 animal discs used in disc research to human lumbar disc: axial compression mechanics and
38 glycosaminoglycan content," *Spine (Phila Pa 1976)*, 33(6), pp. E166-173.
- 39 [32] Heuer, F., Schmidt, H., Klezl, Z., Claes, L., and Wilke, H.-J., 2007, "Stepwise reduction of functional
40 spinal structures increase range of motion and change lordosis angle," *Journal of biomechanics*, 40(2), pp.
41 271-280.
- 42 [33] Markolf, K. L., 1972, "Deformation of the thoracolumbar intervertebral joints in response to
43 external loads: a biomechanical study using autopsy material," *J Bone Joint Surg Am*, 54(3), pp. 511-533.
- 44 [34] Cook, D. J., Yeager, M. S., and Cheng, B. C., 2015, "Range of motion of the intact lumbar segment:
45 a multivariate study of 42 lumbar spines," *International journal of spine surgery*, 9.
- 46 [35] Percy, M., Portek, I., and Shepherd, J., 1984, "Three-dimensional x-ray analysis of normal
47 movement in the lumbar spine," *Spine*, 9(3), pp. 294-297.

- 1 [36] Yamamoto, I., Panjabi, M. M., Crisco, T., and Oxland, T. O. M., 1989, "Three-dimensional
2 movements of the whole lumbar spine and lumbosacral joint," *Spine*, 14(11), pp. 1256-1260 %@ 0362-
3 2436.
- 4 [37] Maas, S. A., Ellis, B. J., Ateshian, G. A., and Weiss, J. A., 2012, "FEBio: finite elements for
5 biomechanics," *Journal of biomechanical engineering*, 134(1), p. 011005.
- 6 [38] O'Connell, G. D., Leach, J. K., and Klineberg, E. O., 2015, "Tissue engineering a biological repair
7 strategy for lumbar disc herniation," *BioResearch open access*, 4(1), pp. 431-445.
- 8 [39] Reitmaier, S., Volkheimer, D., Berger-Roscher, N., Wilke, H.-J., and Ignatius, A., 2014, "Increase or
9 decrease in stability after nucleotomy? Conflicting in vitro and in vivo results in the sheep model," *Journal*
10 *of The Royal Society Interface*, 11(100), p. 20140650.
- 11 [40] Costi, J. C., E., L., and O'Connell, G. D., 2020 - In Review, "Spine Biomechanical Testing
12 Methodologies: The Controversy of Consensus vs Scientific Evidence.," *JOR Spine*, Special Issue: Protocols,
13 *Methods, and Resources for Spine Research*.
- 14 [41] M., Z., Werbner, B., and O'Connell, G. D., 2020 - In Review, "Perspective on combined
15 experimental and computational approaches for investigating annulus fibrosus mechanics," *J Biomech*
16 *Eng*.
- 17 [42] Yang, B., and O'Connell, G. D., 2019, "Intervertebral disc swelling maintains strain homeostasis
18 throughout the annulus fibrosus: A finite element analysis of healthy and degenerated discs," *Acta*
19 *Biomater*, 100, pp. 61-74.
- 20 [43] Tavakoli, J., Amin, D. B., Freeman, B. J., and Costi, J. J., 2018, "The Biomechanics of the Inter-
21 Lamellar Matrix and the Lamellae During Progression to Lumbar Disc Herniation: Which is the Weakest
22 Structure?," *Annals of biomedical engineering*, pp. 1-12.
- 23 [44] Vernon-Roberts, B., Fazzalari, N. L., and Manthey, B. A., 1997, "Pathogenesis of tears of the anulus
24 investigated by multiple-level transaxial analysis of the T12-L1 disc," *Spine*, 22(22), pp. 2641-2646 %@
25 0362-2436.
- 26 [45] Vernon-Roberts, B., Moore, R. J., and Fraser, R. D., 2007, "The natural history of age-related disc
27 degeneration: the pathology and sequelae of tears," *Spine*, 32(25), pp. 2797-2804 %@ 0362-2436.
- 28 [46] Putzier, M., Schneider, S. V., Funk, J. F., Tohtz, S. W., and Perka, C., 2005, "The surgical treatment
29 of the lumbar disc prolapse: nucleotomy with additional transpedicular dynamic stabilization versus
30 nucleotomy alone," *Spine*, 30(5), pp. E109-E114.
- 31 [47] Yorimitsu, E., Chiba, K., Toyama, Y., and Hirabayashi, K., 2001, "Long-term outcomes of standard
32 discectomy for lumbar disc herniation: a follow-up study of more than 10 years," *Spine*, 26(6), pp. 652-
33 657 %@ 0362-2436.
- 34 [48] O'Connell, G. D., Guerin, H. L., and Elliott, D. M., 2009, "Theoretical and uniaxial experimental
35 evaluation of human annulus fibrosus degeneration," *Journal of biomechanical engineering*, 131(11), p.
36 111007.
- 37 [49] Wilke, H. J., Schmidt, H., Werner, K., Schmolz, W., and Drumm, J., 2006, "Biomechanical evaluation
38 of a new total posterior-element replacement system," *Spine (Phila Pa 1976)*, 31(24), pp. 2790-2796;
39 *discussion 2797*.
- 40 [50] Elliott, D. M., Yerramalli, C. S., Beckstein, J. C., Boxberger, J. I., Johannessen, W., and Vresilovic, E.
41 J., 2008, "The effect of relative needle diameter in puncture and sham injection animal models of
42 degeneration," *Spine (Phila Pa 1976)*, 33(6), pp. 588-596.
- 43 [51] Michalek, A. J., Funabashi, K. L., and Iatridis, J. C., 2010, "Needle puncture injury of the rat
44 intervertebral disc affects torsional and compressive biomechanics differently," *Eur Spine J*, 19(12), pp.
45 2110-2116.
- 46 [52] Michalek, A. J., and Iatridis, J. C., 2012, "Height and torsional stiffness are most sensitive to annular
47 injury in large animal intervertebral discs," *The Spine Journal*, 12(5), pp. 425-432.

- 1 [53] Haughton, V. M., Rogers, B., Meyerand, M. E., and Resnick, D. K., 2002, "Measuring the axial
2 rotation of lumbar vertebrae in vivo with MR imaging," *AJNR Am J Neuroradiol*, 23(7), pp. 1110-1116.
- 3 [54] Long, R. G., Burki, A., Zysset, P., Eglin, D., Grijpma, D. W., Blanquer, S. B. G., Hecht, A. C., and
4 Iatridis, J. C., 2016, "Mechanical restoration and failure analyses of a hydrogel and scaffold composite
5 strategy for annulus fibrosus repair," *Acta Biomater*, 30, pp. 116-125.
- 6 [55] Guterl, C. C., See, E. Y., Blanquer, S. B., Pandit, A., Ferguson, S. J., Benneker, L. M., Grijpma, D. W.,
7 Sakai, D., Eglin, D., and Alini, M., 2013, "Challenges and strategies in the repair of ruptured annulus
8 fibrosus," *European cells & materials*, 25, p. 1.
- 9 [56] Gorenssek, M., Jaksimovic, C., Kregar-Velikonja, N., Gorenssek, M., Knezevic, M., Jeras, M., Pavlovic,
10 V., and Cor, A., 2004, "Nucleus pulposus repair with cultured autologous elastic cartilage derived
11 chondrocytes," *Cell Mol Biol Lett*, 9(2), pp. 363-373.
- 12 [57] Nolan, D. R., Gower, A. L., Destrade, M., Ogden, R. W., and McGarry, J. P., 2014, "A robust
13 anisotropic hyperelastic formulation for the modelling of soft tissue," *Journal of the mechanical behavior
14 of biomedical materials*, 39, pp. 48-60.
- 15 [58] Ateshian, G. A., 2007, "On the theory of reactive mixtures for modeling biological growth,"
16 *Biomech Model Mechanobiol*, 6(6), pp. 423-445.
- 17 [59] Vadalà, G., Russo, F., Pattappa, G., Schiuma, D., Peroglio, M., Benneker, L. M., Grad, S., Alini, M.,
18 and Denaro, V., 2013, "The transpedicular approach as an alternative route for intervertebral disc
19 regeneration," *Spine*, 38(6), pp. E319-E324 %@ 0362-2436.

20